International Journal of Heat and Mass Transfer 51 (2008) 5296–5304

Contents lists available at ScienceDirect

International Journal of Heat and Mass Transfer

journal homepage: www.elsevier.com/locate/ijhmt

Interphase transfer at oscillatory rough surfaces

H.G. Gomaa *

Chemical and Biochemical Engineering Department, University of Western Ontario, London, Ontario, Canada N6A 5B9

ARTICLE INFO

Article history:
Received 23 July 2007
Received in revised form 7 March 2008
Available online 16 May 2008

Keywords:
Interphase transfer
Oscillatory motion
Enhancement
Rough surface
Turbulent promoters
Process intensification

ABSTRACT

The interphase transfer at oscillatory rough surfaces have been investigated and an analytical model is developed for predicting the time average transfer rate at surfaces equipped with transverse rectangular roughness elements. The model is based on the theory of isotropic turbulence in which the energy dissipation is determined from solving the equation of oscillatory motion in the boundary layer using time-invariant eddy viscosity. It was found that the combined effect of oscillatory motion and turbulence promoters can result in substantial transfer augmentation at a solid–fluid interface. Such augmentation is mainly attributed to formation of eddies on the downstream side of the roughness element, which upon deceleration and reversal are ejected into the bulk flow. The model predictions agrees satisfactorily with the experimental measurements with correlation coefficient $R = 0.98$.

1. Introduction

Application of oscillatory motion has proven to increase heat and mass transfer rate at fluid–solid interface orders of magnitude greater than that afforded by molecular diffusion alone, thus making it an attractive approach for enhancing the performance of many diffusion-limited processes. This include membrane filtration [1–3], electrochemical reactions [4,5], as well as heat-pumping applications where significant heat transfer enhancement is achieved when oscillatory motion is combined with axial temperature gradient as demonstrated by Kurzweg [6–8]. The fact that achieving high transfer rates is practically de-coupled from process flow conditions is another advantage of using oscillatory motion since process flows and consequently residence time can be controlled independently. This feature is useful in medical and biochemical engineering applications where viscous shear sensitive material does not allow operating under turbulent flow conditions [9,10].

The magnitude of enhancement associated with the velocity vector created by periodic excitation of the liquid or the surface is a function of the fluid dynamics and characteristics in the boundary layer and many efforts have been directed toward understanding the conditions that destabilize the layer to create turbulence. The results of such investigations showed that turbulence and enhancement are highest when oscillatory motion was combined with flow separation induced by surface modifications such as turbulence promoters (TP), as shown by Gomaa and Al-Taweel [11], grooves as demonstrated by Herman and Kang [12,13], and baffles used by Mackley and co-workers [14,15].

Although many studies has been conducted on the subject and its potential applications in process intensification, there is still a gap in understanding the relation between the enhancement mechanism and the flow field developed by the interaction of the oscillatory motion and TP. For example, while some authors attributed performance improvement to the formation of standing vortex wave [16–18], others reported that much of it, if not most, is due to the negative pressure portion generated each half of the oscillatory cycle [19–21]. Both mechanisms, on the other hand, are different from self-sustained resonant transport [22,23]. Also, differences in TP design and effectiveness has been reported by several investigators, such as Yoshida et al. [24] who recommended using semi-cylindrical promoters with 30° angle, as compared to Bellhouse and co-workers [3] who used helical flow passages. Both designs on the other hand were found to be less effective than winding or Kenics inserts in terms of energy efficiency and transfer enhancement as reported by Xu et al. [25] and Krstic et al. [26], respectively.

The objective of this work is to address some of the issues mentioned above and to gain better understanding of the fluid mechanics and transfer characteristics at solid–fluid interface under the combined effect of oscillatory motion and TP. Another objective is to develop an analytical model for describing such conditions to enable proper design and scale up methodology for the effective use of technique. The model predictions will then be compared with experimental measurements to validate its accuracy.

* Tel.: +1 519 661 3498; fax: +1 519 661 2111x81274.
E-mail address: Hgomaa@uwo.ca

0017-9310/$ - see front matter © 2008 Elsevier Ltd. All rights reserved.
doi:10.1016/j.ijheatmasstransfer.2008.03.011

Nomenclature

a	oscillation amplitude (mm)
A	active surface area (mm^2)
A_f	total frontal area of roughness element (mm^2)
A_s	windward wetted area of roughness element (mm^2)
B	constant, Eq. (42) (–)
C	constant, Eq. (43) (–)
C_b	concentration of the ferri-ferrocyanide (mol/mm^3)
D	diffusion coefficient (mm^2 s^{-1})
F	Faraday's constant (C/equiv.)
f	oscillation frequency (Hz)
f_s	friction factor (–)
h	promoter height (mm)
h_s	Nikuradse equivalent sand roughness (mm)
i	limiting current (C/s)
J	dimensionless variable Eq. (24c) (–)
k	mass transfer coefficient (mm s^{-1})
L	plate length (mm)
n	number of electrons transferred in the reaction (–)
p	promoters spacing (mm)
Re_{os}	Reynolds number, ($Re_{os} = \frac{a\omega L}{\nu}$) (–)
Wo	Womersley number, ($Wo = L\sqrt{\frac{\omega}{\nu}}$) (–)
S	area of smooth surface without promoters (mm^2)
S_f	total frontal area (mm^2)
Sc	Schmidt number, ($Sc = \nu/D$) (–)
Sh_{os}	Sherwood number, oscillatory condition ($Sh_{os} = kL/D$) (–)
Sh_n	Sherwood number, natural convection (–)
t	time (s)
u, v, w	x-, y-, z-velocities in the boundary layer, respectively (mm s^{-1})
$\bar{u}, \bar{v}, \bar{w}$	mean component of u, v, w, respectively (mm s^{-1})
u', v', w'	fluctuating components of u, v, w, respectively (mm s^{-1})
U	fluid oscillation velocity outside the boundary layer (mm s^{-1})
U_0	velocity oscillation amplitude outside the boundary layer (mm s^{-1})
u_m	velocity oscillation amplitude inside the boundary layer (mm s^{-1})
u_f	frictional velocity, Eq. (20) (mm s^{-1})

Greek symbols

β	wall layer constant, Eq. (34) (–)
γ	Euler number (0.5772)
δ_l	laminar boundary layer thickness (mm)
δ_t	turbulent boundary layer thickness (mm)
λ	roughness density, Eq. (47) (–)
ν	kinematic viscosity (mm^2 s^{-1})
η_l	dimensionless variable, laminar flow Eq. (14) (–)
η_t	dimensionless variable, turbulent flow Eq. (35) (–)
ε_t	eddy viscosity (mm^2 s^{-1})
κ	Karman constant (0.4) (–)
ρ	fluid density (g mm^{-3})
τ_l	laminar shear stress [g mm^{-1} s^{-2})
τ	total shear stress (g mm^{-1} s^{-2})
τ_0	shear rate at the solid–liquid interface (g mm^{-1} s^{-2})
τ_t	Reynolds stress (g mm^{-1} s^{-2})
ζ, ζ_0	dimensionless parameters, Eqs. (24a,b) (–)
ψ	specific energy dissipation per unit mass, Eq. (27) (mm^2 s^{-3})
ω	circular frequency of oscillation, $2\pi f$ (s^{-1})

2. Theoretical analysis

2.1. Background

The subject of diffusion across unsteady laminar boundary layer has been addressed by several investigators where both numerical and analytical solutions have been developed for wide range oscillatory conditions, and a good review of the subject has been given by Gomaa and Al-Taweel [27]. Under conditions of modified surface geometry the situation is much more complex due the separation and reattachment of the boundary layer which varies in time and space by both the specific surface geometry and the oscillatory conditions, and most investigators have applied numerical approaches to analyze the problem.

Sobey [28,29] numerically analyzed the flow oscillation in a wavy- walled channel to explain the high mass transfer rate achieved earlier in the membrane oxygenator developed by Bellhouse et al. [30], and attributed the enhancement to a vortex formation–ejection cycle. Howes et al. [31] numerically simulated the flow in a baffled channel, and showed that the presence of chaotic flow pattern under oscillatory flows provided efficient mixing and resulted in high interface solid–fluid transfer rates. Wang et al. [32] numerically simulated cross-flow filtration in baffled tubular channels under pulsating flow and concluded that flow pulsation significantly enhanced the membrane flux and reduced the wall concentration.

Nishimura et al. [33] studied flow and mass transfer characteristics in sinusoidal wavy-walled channels for pulsating flows and showed that mass transfer enhancement increased with both Reynolds and Strouhal numbers. Latter on, Nishimura and Matsune [34] attributed the mass transfer enhancement there to the vortex expansion and shrinkage in each furrow of the channel during the deceleration and acceleration phase of the oscillatory cycle. Recently, Nishimura et al. [35,36] compared experimentally the flow characteristics in wavy-walled channel and wavy-walled tube, and showed that the resonant transport enhancement, attributed to the Tollmien–Schlichting waves, does not exist in a wavy-walled tube, in contrast to a wavy-walled channel.

In recent work, Nagaoka et al. [37] modeled numerically mass transfer to filamentous biofilm under oscillatory flow conditions using *low Reynolds number* k–ϵ turbulence model. Comparison of the measured and calculated results indicated that mass transfer mechanism between the fluid and the surface is mainly attributed to turbulent diffusion caused by flow oscillation over the rough filamentous surface. This was found to be consistent with the work of Rama Rao and Baird [38], who correlated heat transfer data in reciprocating plate column using turbulence energy dissipation concept.

2.2. Model development

Assuming a surface placed in a fluid oscillating harmonically with velocity U given by

$$U = U_0 e^{iwt}, \tag{1}$$

where U_0 is the maximum velocity amplitude ($U_0 = aw$), a the oscillation amplitude, and ω the angular oscillation frequency. Under such conditions, and taking the x in axes the direction of oscillation, while y and z at right angles and parallel perpendicular to it, respectively, the Navier–Stokes and the continuity equations are

$$\frac{\partial(u-U)}{\partial t}+u\frac{\partial u}{\partial x}+v\frac{\partial u}{\partial y}+w\frac{\partial u}{\partial z}=\nu\nabla^2 u, \tag{2}$$

$$\frac{\partial u}{\partial x}+\frac{\partial v}{\partial y}+\frac{\partial w}{\partial z}=0, \tag{3}$$

where u, v, and w are the velocity components in the x, y, and z directions, respectively, and ν is the kinematic viscosity of the fluid. Expressing the velocity in terms of its *mean* and *fluctuating* components and substitution into the continuity equation,

$$\frac{\partial\bar{u}}{\partial x}+\frac{\partial\bar{v}}{\partial y}+\frac{\partial\bar{w}}{\partial z}+\frac{\partial u'}{\partial x}+\frac{\partial v'}{\partial y}+\frac{\partial w'}{\partial z}=0. \tag{4}$$

Taking the time-averaged value of Eq. (5), and keeping in mind that u', v', and w' averaged in the x, and z directions, are zero, we get

$$\frac{\partial\bar{u}}{\partial x}+\frac{\partial\bar{v}}{\partial y}+\frac{\partial\bar{w}}{\partial z}=0. \tag{5}$$

Similarly, substitution of the velocity components into the Navier–Stokes equation and performing the time-averaging process we obtain,

$$\frac{\partial(\bar{u}-U)}{\partial t}+\bar{u}\frac{\partial\bar{u}}{\partial x}+\bar{v}\frac{\partial\bar{u}}{\partial y}+\bar{w}\frac{\partial\bar{u}}{\partial z}=\nu\nabla^2\bar{u}\frac{\partial(\overline{u'^2})}{\partial x}+\frac{\partial(\overline{u'v'})}{\partial y}+\frac{\partial(\overline{u'w'})}{\partial z}. \tag{6}$$

Assuming that the flow is homogenous in the x and z directions such that the ensemble averaged quantities are independent of x and z, then,

$$\frac{\partial\bar{u}}{\partial x}=\frac{\partial\bar{u}}{\partial z}=0,\quad \bar{v}=0,\quad \bar{w}=0 \tag{7}$$

Substitution in (6), we get

$$\frac{\partial(\bar{u}-U)}{\partial t}=\frac{\partial}{\partial y}\left\{\nu\frac{\partial\bar{u}}{\partial y}-\overline{u'v'}\right\}. \tag{8}$$

The right hand side of Eq. (8) represents the total stress τ as the sum of the laminar τ_l, and turbulent or Reynolds stresses τ_t, respectively,

$$\frac{\tau_l}{\rho}=\nu\frac{\partial\bar{u}}{\partial y}, \tag{9}$$

$$\frac{\tau_t}{\rho}=-\overline{u'v'}, \tag{10}$$

where ρ is the liquid density. Using the eddy viscosity ε_t in Eq. (10),

$$\frac{\tau_t}{\rho}=\varepsilon_t\frac{\partial\bar{u}}{\partial y}. \tag{11}$$

Substitution of (10) and (11) into (8) yields,

$$\frac{\partial(\bar{u}-U)}{\partial t}=\frac{\partial}{\partial y}\left[\nu\frac{\partial\bar{u}}{\partial y}+\varepsilon_t\frac{\partial\bar{u}}{\partial y}\right]. \tag{12}$$

For a smooth surface, the boundary conditions applied to Eq. (12) are,

$$\bar{u}=0\quad \text{at } y=0, \tag{13a}$$

$$\tau\to 0\quad \text{as } y\to\delta. \tag{13b}$$

In the case of *laminar* oscillatory motion, the velocity fluctuation components vanish and the eddy viscosity is zero leading to the well known Stokes solution [39] given by

$$u=U_0[\cos\omega t-e^{-\eta}\cos(\omega t-\eta)],\qquad \eta=y\sqrt{\frac{\omega}{2\nu}}. \tag{14}$$

The corresponding laminar boundary layer thickness δ_l is then,

$$\delta_l=\pi\sqrt{\frac{\nu}{2\omega}}. \tag{15}$$

For rough surfaces, the virtual or Reynolds stress far outweighs the viscous components and the latter may be omitted in Eq. (12) with a good degree of approximation leading to,

$$\frac{\partial(\bar{u}-U)}{\partial t}=\frac{\partial}{\partial y}\left[\varepsilon_t\frac{\partial\bar{u}}{\partial y}\right]. \tag{16}$$

Furthermore, the boundary conditions (13a) for the case of rough surface is,

$$\bar{u}=0\quad \text{for } y=y_0, \tag{17}$$

where y_0 is the "*hydrodynamic roughness*", which is a mathematical construct defined as the height at which the velocity profile would go to zero if extrapolated towards the boundary, and is given by Nikuradse [40],

$$y_0=h_s/30, \tag{18}$$

where h_s is the Nikuradse equivalent roughness, which relates the effect of actual roughness geometry to that of closely packed sand grains under the same flow conditions [41]. Assuming the eddy viscosity to be time independent and applying Prandtl's mixing length theory, ϵ_t can be expressed by

$$\varepsilon_t=\kappa u_f y, \tag{19}$$

where κ is the Von Karman constant (=0.41) and u_f the maximum friction velocity defined in terms of the maximum shear stress τ_0 or the friction factor f_s by,

$$u_f=\sqrt{\frac{\tau_0}{\rho}}=\sqrt{\frac{f_s}{2}}U_0. \tag{20}$$

By expressing the velocity profile in a complex form,

$$(\bar{u}-U)=u_m e^{iwt}, \tag{21}$$

where m denotes velocity amplitude, Eq. (16) can be written with the aid of Eqs. (19) and (21) as,

$$\frac{\partial}{\partial y}\left[\frac{\kappa u_f}{\omega}y\frac{\partial u_m}{\partial y}\right]-iu_m=0. \tag{22}$$

Solution of Eq. (22) with boundary conditions (17) can be expressed in terms of *Kelvin* functions ker, and kei in the form,

$$u_m=U_0\sqrt{\frac{(\ker\zeta_0-\ker\zeta)^2+(\mathrm{kei}\zeta_0-\mathrm{kei}\zeta)^2}{\ker^2\zeta_0-\mathrm{kei}^2\zeta_0}}, \tag{23}$$

where ζ, ζ_0, and J are defined by,

$$\zeta=2\sqrt{\frac{y}{\kappa h_s J}}, \tag{24a}$$

$$\zeta_0=\frac{2}{\sqrt{30\kappa J}}, \tag{24b}$$

$$J=\frac{u_f}{h_s\omega}. \tag{24c}$$

Using the above, the maximum shear stress τ_0 and the friction factor f_s can be expressed by,

$$\tau_0=\left.\frac{\partial\bar{u}}{\partial y}\right|_{y=0}=\rho\frac{\kappa}{2}u_f U_0\zeta_0\sqrt{\frac{(\ker'\zeta_0)^2+(\mathrm{kei}'\zeta_0)^2}{\ker^2\zeta_0+\mathrm{kei}^2\zeta_0}}, \tag{25}$$

$$f_s=\frac{\kappa^2}{2}\zeta_0^2\frac{(\ker'\zeta_0)^2+(\mathrm{kei}'\zeta_0)^2}{\ker^2\zeta_0+\mathrm{kei}^2\zeta_0}. \tag{26}$$

For small ζ_0 values, (*small* $h_{(s)}$, *Kelvin* functions can be approximated by,

$$\ker x=-\ln\left(\frac{x}{2}-e^{\gamma}\right)+O(x^2)\quad(\gamma:\ \text{Euler number}=0.5772\ldots), \tag{27a}$$

$$\mathrm{kei}\,x=-\frac{\pi}{4}+O(x^2\ln x), \tag{27b}$$

$$\ker' x = -\frac{1}{x}(1 + O(x^2)), \tag{27c}$$

$$\mathrm{kei}' x = \frac{1}{x}(0 + O(x^2 \ln x)). \tag{27d}$$

Substitution of Eqs. (27a–d) into Eqs. (23), (25) and (26), we find,

$$u_m = \frac{u_f}{\kappa} \ln\left(\frac{30z}{h_s}\right), \tag{28}$$

$$\tau_0 = \frac{\rho U_0^2 \kappa^2}{\ln^2(30\kappa e^{-2\gamma} J)}, \tag{29}$$

$$f_s = \frac{2\kappa^2}{\ln^2(30\kappa e^{-2\gamma} J)}. \tag{30}$$

Since at the edge of the boundary layer, $y = \delta$ and the velocity amplitude $u_m = U_0$, Eq. (28) yields,

$$U_0 = \frac{u_f}{\kappa} \ln\left(\frac{30\delta}{h_s}\right). \tag{31}$$

Substitution of Eq. (20) for u_f into Eq. (30) gives,

$$f_s = \frac{2\kappa^2}{\ln^2\left(\frac{30\delta}{h_s}\right)}. \tag{32}$$

By comparing (32) with (30) one finds that,

$$\delta = h_s \kappa e^{-2\gamma} J. \tag{33}$$

For surfaces with "large" roughness (*large* h_s), the eddy viscosity is dominated by the surface roughness, and Eq. (19) is substituted by,

$$\varepsilon_t = \beta u_f h_s, \tag{34}$$

where β is the "wall layer proportionality constant" that needs to be determined. Using Eq. (34), solution to Eq. (12) can simply be expressed by the same form given in Eq. (14) by replacing the kinematic viscosity ν by the eddy viscosity ϵ_t,

$$\begin{aligned} &\bar{u} = U_0[\cos\omega t - \mathrm{Exp}^{-\eta_t}\cos(wt - \eta_t)], \\ &\eta_t = y\sqrt{\frac{\omega}{2\varepsilon_t}}. \end{aligned} \tag{35}$$

Similarly, the boundary layer thickness can be given in terms of the eddy viscosity as,

$$\delta = \pi\sqrt{\frac{\varepsilon_t}{2\omega}} = \frac{\pi h_s}{4}\sqrt{\beta J}. \tag{36}$$

Using (35), the amplitude of the oscillation velocity u_m can be expressed by,

$$u_m = U_0\sqrt{1 + e^{-2\eta_t} - 2e^{-\eta_t}\cos(\eta_t)}. \tag{37}$$

Also, the maximum shear stress τ_0 and the friction factor f_s can be obtained,

$$\tau_0 = \left.\frac{\partial \bar{u}}{\partial y}\right|_{y=0} = \sqrt{2}\rho\beta h_s U_0 u_f \eta_t, \tag{38}$$

$$f_s = \frac{2}{U_0^2}\left(\frac{\tau_0}{\rho}\right) = \frac{2\beta}{J}. \tag{39}$$

The value of β can be determined by matching f_s and δ determined for small and large h_s values. Thus, combining Eqs. (32) and (39) for f_s yields,

$$\frac{2\beta}{J} = \frac{2\kappa^2}{\ln^2(30\kappa e^{-2\gamma} J)}. \tag{40}$$

Similarly, matching Eqs. (33)–(36) for δ gives,

$$\frac{\pi}{4}\sqrt{\beta J} = \kappa e^{-2\gamma} J. \tag{41}$$

Solving Eqs. (40) and (41) gives $\beta = .0812$.

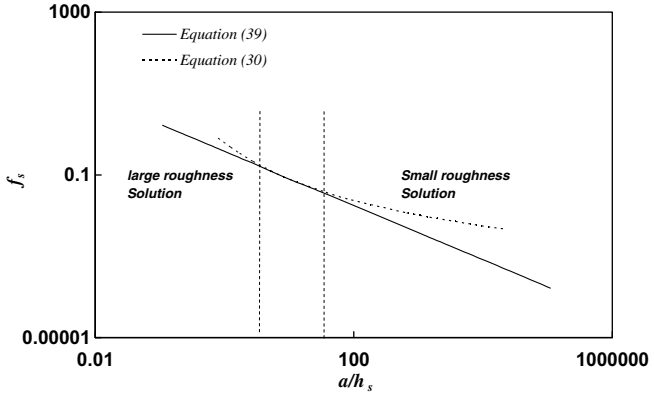

Fig. 1. Comparison between "*large roughness*", and "*small roughness*" solutions.

Fig. 1 shows the friction factor f_s as a function of a/h_s estimated using both Eqs. (30) and (39) for small and large h_s values, respectively. It can be seen that for $a/h_s < 5$ the large roughness solution is applicable, while for $a/h_s > 30$, small roughness analysis is more applicable.

2.3. Estimation of h_s

The Nikuradse equivalent sand roughness h_s for a particular surface configuration can be determined using the Nikuradse data for sand roughness and the equation describing turbulent flow given by,

$$\frac{u}{u_f} = \frac{1}{\kappa}\ln\frac{u_f y}{\nu} + B, \tag{42}$$

where B is a constant equals 5.8 for turbulent flow over flat surface. For the case of rough surface, Nikuradse [40] established that the effect of roughness is a shift of the logarithmic profile in Eq. (42) represented by an additional term (given in brackets) as,

$$\frac{u}{u_f} = \frac{1}{\kappa}\ln\frac{u_f y}{\nu} + B - \left\{\frac{1}{\kappa}\ln\frac{u_f h}{\nu} + C\right\}, \tag{43}$$

where h is the height of the roughness elements, and C is a function of the geometry, density, and the arrangement of the roughness elements. For conditions of sand roughness where h equals h_s, Nikuradse determined that $C = -3.0$, thus, substitution into Eq. (43) gives,

$$\frac{u}{u_f} = \frac{1}{\kappa}\ln\frac{u_f}{\nu} + B - \left\{\frac{1}{\kappa}\ln\frac{u_f h_s}{\nu} - 3\right\}. \tag{44}$$

Combining Eqs. (43) and (44) then yields,

$$h_s = h\mathrm{Exp}[\kappa(3.0 + C)]. \tag{45}$$

Several authors have attempted to correlate the term C in Eq. (45) with roughness density, and general approach was suggested in which transverse roughness were classified into two types: k-type, and d-type where the letters "k" and "d" denote the significant length scale that determines the roughness function, velocity profiles, and friction factor. Tani [42] suggested that, for regularly spaced ribs, a demarcation between the two types might be set at a pitch ratio $p/h = 4$, where p, is the spacing between two adjacent roughness elements, and h is its height. For d-type roughness typified by closely spaced ribs with p/h less than 4, the ribs are so closely spaced and the roughness function is independent of the size of the roughness with stable vortices set in the grooves and negligible eddy shedding from the roughness elements into the outer flow which remains relatively undisturbed by the roughness elements. For the k-type roughness typified by sparsely spaced transverse ribs with p/h greater than 4, eddies with length scale

of the roughness height are shed from the roughness elements and penetrate into the bulk flow toward the boundary layer edge, and the roughness function and friction factor depend on the size of the roughness element.

For the strip type transverse promoters used in this work, the correlation of Sigal and Danberg [43] for determining h_s using the roughness density parameter λ will be applied,

$$h_s = h\begin{cases} 0.00321\lambda^{4.925} & 1.4 \leqslant \lambda \leqslant 4.89 \\ 8.0 & 4.89 \leqslant \lambda \leqslant 13.25 \\ 151.71\lambda^{-1.1379} & 13.25 \leqslant \lambda \leqslant 100.0 \end{cases}, \tag{46}$$

$$\lambda = \frac{S}{S_f}\left(\frac{A_f}{A_s}\right)^{-1.6}, \tag{47}$$

where S is the area of the smooth surface before adding the roughness, S_f, the total frontal area, A_f, frontal area of an element, and A_s, the windward wetted surface area.

2.4. Mass transfer coefficient

Calderbank and Moo-Young [44] invoked the Kolmogoroff theory of isotropic turbulence in their discussion of turbulent heat and mass transfer, and suggested that a general law operates to relate energy dissipation and the specific rates of transport processes in any turbulent flow system. Latter, Kawase and Moo-Young [45] derived a theoretical model for interphase solid–fluid turbulent heat and mass transfer using a combination of the Levich three-zone model, and the Kolmogoroff theory of isotropic turbulence. The model, unified by introducing the energy dissipation rate, was found applicable in describing many systems involving turbulent transport. Accordingly, expression for the mass transfer coefficient was given by,

$$k = 0.134Sc^{-\frac{2}{3}}(\psi\nu)^{\frac{1}{4}}, \tag{48}$$

where ψ is the specific energy dissipation rate per unit mass of the fluid and Sc is the Schmitt number defined as the ratio of the kinematic viscosity ν and the molecular diffusivity D,

$$Sc = \frac{\nu}{D}. \tag{49}$$

For the case of the oscillating surface considered in this analysis, ψ can be expressed in the following form,

$$\psi = \tau_0\bar{u}/h_s\rho. \tag{50}$$

For the experimental and surface roughness conditions used in this investigations, a/h_s values were found to be <4.8. Therefore, $\bar{u}$ and τ_0 are determined using *large roughness* analysis given by Eqs. (35) and (38). Substitution in Eq. (50) and averaging over one cycle,

$$\psi = \frac{2}{3\pi h_s}\sqrt{\varepsilon_t}\left[a^2\omega^{\frac{5}{2}}\right]. \tag{51}$$

Using (51) and rearranging, Eq. (48) can be expressed in terms of the dimensionless Sherwood number for oscillatory conditions Sh_{os} as,

$$Sh_{os} = 0.5\left[\frac{a}{h_s}\sqrt{\frac{f_s}{2}}\right]^{\frac{1}{8}}(Re_{os}Wo)^{\frac{1}{2}}Sc^{\frac{1}{3}}, \tag{52}$$

where

Sh_{os}, Sherwood number,

$$Sh_{os} = \frac{kL}{D}, \tag{52a}$$

Re_{os}, Reynolds number,

$$Re_{os} = \frac{a\omega L}{\nu}, \tag{52b}$$

Wo, Womersley number,

$$Wo = L\sqrt{\frac{\omega}{\nu}}. \tag{52c}$$

3. Results and discussion

3.1. Measurement of time average mass transfer coefficient

Eqs. (48)–(52) were used to calculate the mass transfer rate at oscillating surfaces equipped with turbulence promoters. To validate the proposed analysis, the estimated values are compared to those measured experimentally for wide range of oscillatory parameters and surface configurations (Table 1) using the limiting current technique for the electrochemical redox reaction of ferri-ferrocyanide given by,

$$Fe(CN)_6^{3-} + e^- \leftrightarrows Fe(CN)_6^{4-}.$$

The above system was selected for its fast electron transfer kinetics and for maintaining constant concentration throughout the experiment, since ferricyanide is reduced to ferrocyanide at the cathode surface while the reverse occurs at the anode surface. At the limiting current conditions, the concentration of the ferricyanide is reduced to virtually zero at the cathode surface, and the time average mass transfer coefficient k, can therefore be calculated from,

$$k = \frac{i}{AnFC_b}, \tag{53}$$

where i is the limiting current, A the active mass transfer area, n the number of electrons transferred in the electrochemical reaction, F the Faraday's constant, and C_b the electrolyte bulk concentration.

The experimental setup used is schematically shown in Fig. 2a. It consists of three main subsections: an electrolytic cell, an oscillatory motion mechanism, and a power supply and current measurement system. The cell consisted of 30 l rectangular Plexiglas tank filled with 0.01 mol potassium ferri-ferrocyanide in a two molar sodium hydroxide solution. The cell was covered with black plastic film to protect against photochemical decomposition of the electrolyte. The container cover was designed to hold a reference probe, a nitrogen sparger, a thermometer, and was equipped with a special opening to allow for the free movement of the working electrode. To reduce the effect of dissolved oxygen, freshly prepared solutions were purged with oxygen-free nitrogen for 12 h before its use. Moreover, nitrogen purge was also applied for half an hour before the start of any experiment to de-oxygenate the headspace. To ensure chemical composition stability, a new solution was prepared weekly, and the concentration was checked as per standard procedures at the beginning and at the end of each week. Princeton Applied Research Corp. potentiostat was used to set and maintain the potential difference between the cathode and the solution, and to measure the average current.

The anode was made of a 280 × 240 mm^2 nickel sheet attached to one of the cell walls. Two different sizes polished nickel sheets cathodes (50 × 30 mm^2 and 130 × 30 mm^2) were used. The cathodes were embedded into a 50 mm Plexiglas carrier plate in a fashion that ensured the absence of surface deformity. The leading

Table 1
Experimental conditions

Oscillation amplitude (mm)	0, 5, 10, 20
Oscillation frequency (Hz)	0, 5, 10, 15, 20
Promoters spacing (mm)	8, 16, 24
Promoters height (mm)	1, 2
Plate length (mm)	50, 130

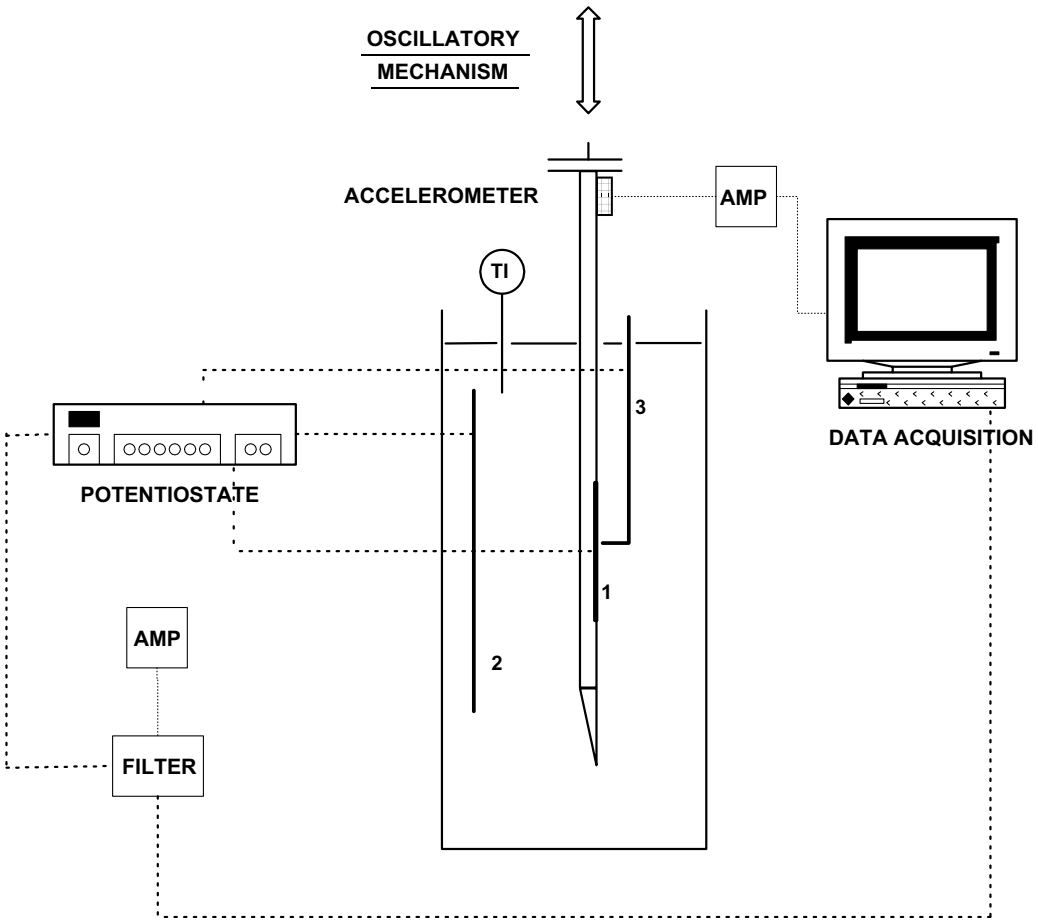

Fig. 2a. Experimental setup: 1 cathode; 2 anode and 3 counter electrode.

edge of the carrier plate was tapered to eliminate streaming and eddy generation at the leading edge. This was further minimized by placing the active cathode surface at least 50 mm away from the leading edge. Two perpendicular ribs were also added to the back of the carrier plate in order to eliminate the onset of lateral vibrations. The cathode was positioned vertically in the middle of the cell between two partitions specially designed to minimize additional streaming. A nickel rod was used as counter electrode, and was located at the mid-height of the cathode. Due to the high conductivity of the electrolyte, changing the probe's position was found to have no effect on the average current density.

Two different promoters heights (1 mm and 2 mm) were used in this investigation Fig. 2b. Both were made of 1 mm thick and 42.5 mm wide smooth rectangular Plexiglas strips glued to the Plexiglas part of the cathode carrier. For each height, three different promoters spacing (8, 16, and 24 mm) were investigated. The promoters were placed on the electrode surface starting at 10 mm above the edge of the active area.

The oscillatory motion was generated using an adjustable eccentric driven by a variable speed motor. This arrangement allowed for a wide range of oscillatory conditions (f = 0–20 Hz, and a = 0–20 mm), which was monitored using an accelerometer attached to the drive shaft and connected to the data acquisition system after passing through a high frequency filter to validate its sinusoidal characteristics.

3.2. Experimental procedure

In order to enhance the reproducibility of results, and to maintain uniform surface conditions, for each experiment, the cathode surface was polished with fine grade emery paper and treated cathodically in a 5% NaOH solution at a current density of 20 mA/cm^2 for about 15 min to allow for hydrogen evolution and surface activation, followed by rinsing with distilled water before placing it into the cell. Similarly, the anode was cleaned with fine emery paper and rinsed with distilled water before using it in the cell. This resulted in decreasing the reproducibility error to within ±3%.

Experiments were conducted at 25 ± 0.5 °C using a potentiostatic approach (at a cell potential of 500 mV). This potential lies approximately at the midpoint of the plateau zone of the current–voltage curve. For each surface height the steady state limiting current was measured under stationary smooth surface conditions to determine the free convective mass transfer coefficient for that particular height. The same was repeated for the stationary surface with promoters. The effect of vibration on the limiting current was then measured for a range of vibrational frequencies at particular amplitudes for the surface with turbulent promoters.

3.3. Effect of oscillatory motion

As indicated in the present analysis, the presence of a relative oscillatory motion at fluid–solid interface equipped with surface irregularities such as transverse TP, generates eddies on the downstream side of the roughness element, which upon deceleration and reversal are ejected into the bulk flow resulting in significant transfer augmentation. An example of the predicted magnitude of such enhancement is shown in Fig. 3 as the ratio of the dimensionless mass transfer coefficient under oscillatory conditions to that at smooth stationary surface due to natural convection. As can be

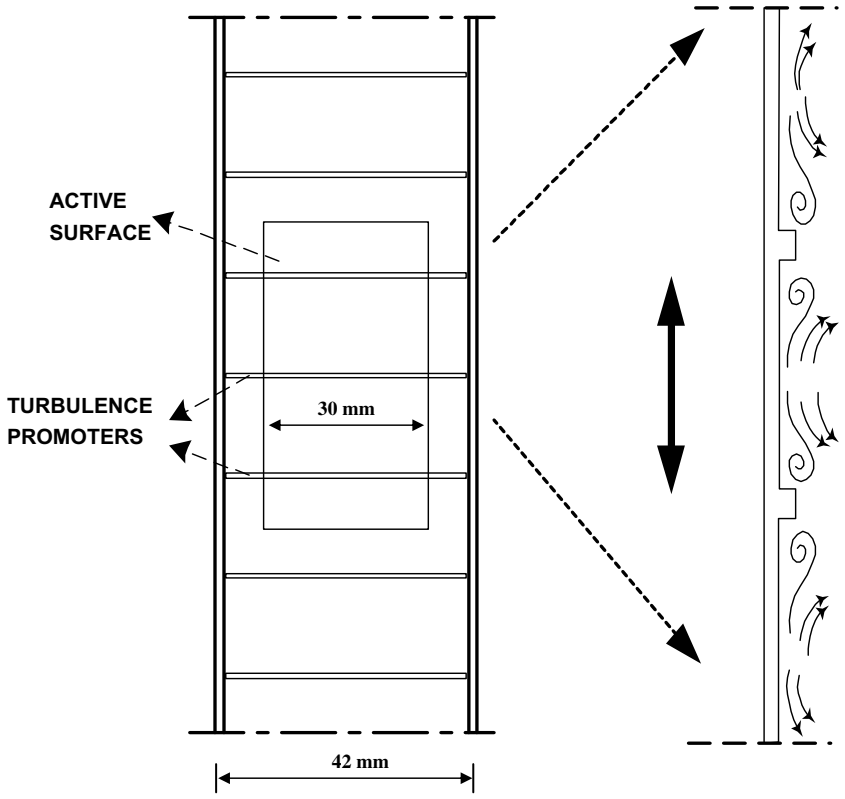

Fig. 2b. Turbulence promoters configuration.

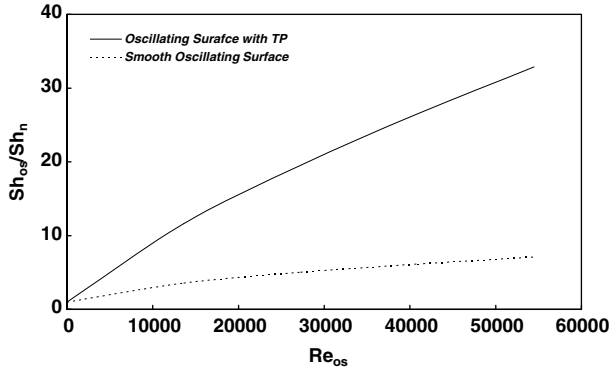

Fig. 3. Effect of turbulence promoters on mass transfer under oscillatory conditions.

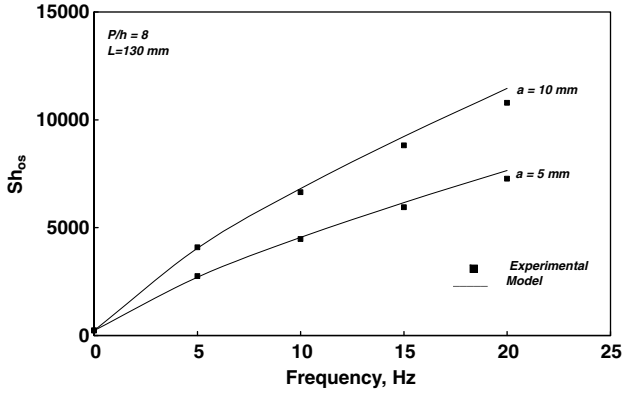

Fig. 4. Effect of oscillation frequency on the mass transfer.

seen, oscillating a surface with 1 mm height rectangular promoters spaced 8 mm apart at frequency f = 10 Hz, and amplitude a = 5 mm results in a mass transfer enhancement of ~20. This is almost four folds the enhancement achieved at a smooth surface oscillating at the same frequency and amplitude. Such enhancement increases with increasing the oscillation frequency and amplitude as shown in Fig. 4, where it can be seen that the model predictions agrees fairly well with the experimental measurements. Similarly, and as shown in Fig. 5, the predicted effect of TP spacing on the rate of mass transfer are also in good agreement with the experimental data. Such good agreement when combined with the fact that the present analysis assumes the effect of natural convection on the time average transfer coefficient to be negligible, further asserts the assumption that the combined effect of TP and oscillatory motion disrupts the natural convection boundary layer to the extent that it becomes no longer a contributor to the transfer mechanism.

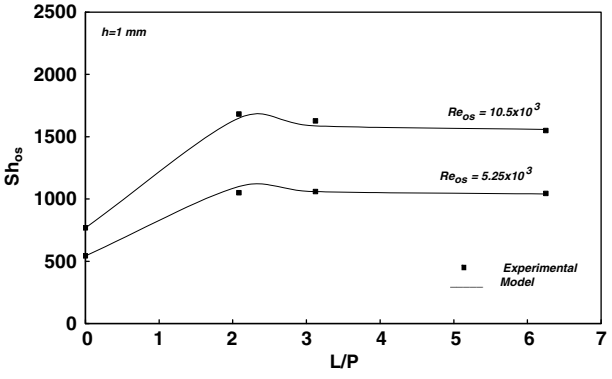

Fig. 5. Effect of number of promoters on mass transfer.

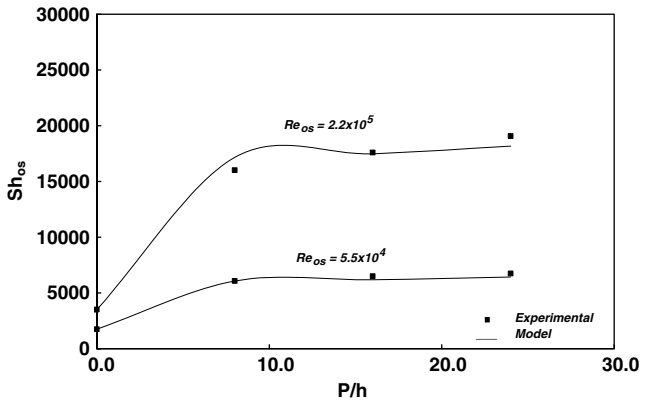

Fig. 6. Effect of prompters spacing to height ratio on mass transfer.

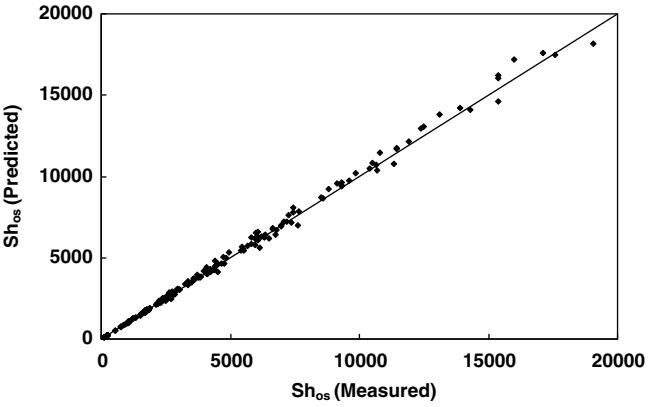

Fig. 7. Comparison between model predictions and experimental data.

In studies of heat and mass transfer at non-oscillatory surfaces under turbulent flow conditions, it was found that increasing the number of promoters beyond a certain value had small or negative effect on transfer augmentation [46–48]. According to these investigations it was shown that for small p/h values, the elements were closely spaced and stable vortices were set up in the spacing between the adjacent elements such that the flow skimmed over the surface and never reattached again resulting in negligible eddy shedding and little transfer enhancement. As p/h increased, the promoters became more sparsely spaced such that eddies were shed from the elements and penetrated into the bulk flow toward the boundary layer edge, causing a much higher transfer rate. Fig. 6 shows similar predictions of the effect of p/h on the mass transfer rate, with the difference that, for steady flow conditions, and as reported in most of the investigations, a decline in transfer rate is observed as p/h continued to increase due to the re-establishment of a boundary layer in the space between the adjacent promoters. Such behaviour is not predicted according to the present analysis and agrees fairly well with the experimental observations.

Fig. 7 shows a general comparison between the model predictions the experimental measurements. It can be seen that the entire set of experimental data are satisfactorily correlated using Eq. (48) with correlation coefficient $R = 0.98$.

4. Conclusions

1. The combined effect of oscillatory motion and turbulence promoters can result in substantial mass transfer augmentation at a solid–fluid interface. Such augmentation is mainly attributed to formation of eddies on the downstream side of the roughness element, which upon deceleration and reversal are ejected into the bulk flow resulting in significant transfer augmentation.
2. A model has been developed for accurately predicting the time average mass transfer at surfaces equipped with transverse rectangular roughness elements. The model is based on theory of isotropic turbulence in which the energy dissipation is determined from solving the equation of oscillatory motion in the boundary layer by assuming time-invariant eddy viscosity.
3. Two solutions were presented based on the ratio of the oscillation amplitude to surface roughness a/h_s. For $a/h_s < 5$, "*large roughness*" solution applies, while for $a/h_s > 36$, a "*small roughness*" solution is more accurate. The experimental conditions used in this investigation correspond to $a/h_s < 5$, therefore, the "*large roughness*" solution was used in comparing the predicted to the measured values.
4. This analysis provides information on the time average value of the transfer coefficient, but does not analyze the instantaneous state of turbulence or how it is related to the time average transfer values.

Acknowledgements

The authors would like to thank the Natural Sciences and Engineering Research Council of Canada for the financial support.

References

[1] P.N. Blanpain-Avet, Doubrovine, C. Lafforgue, M. Lalande, The effect of oscillatory flow on crossflow microfiltration of beer in a tubular mineral membrane system-membrane fouling resistance decrease and energetic considerations, J. Membr. Sci. 152 (1999) 151–174.
[2] S. Najarian, B.J. Bellhouse, Effect of oscillatory flow on the performance of a novel cross-flow affinity membrane device, Biotech. Prog. 13 (1997) 113–116.
[3] B.J. Bellhouse, I.J. Sobey, S. Alani, B.M. DeBlois, Enhanced filtration using flat membranes and standing vortex waves, Bioseparation 4 (1994) 127–138.
[4] H.G. Gomaa, A.M. Al-Taweel, J. Landau, Mass transfer enhancement at vertically oscillating electrodes, Chem. Eng. J. 97 (2004) 141–149.
[5] V. Perez-Herranz, J. Garcia-Anton, J.L. Guinon, Velocity profiles and limiting current in an electrodialysis cell in pulsed flow, Chem. Eng. Sci. 52 (5) (1998) 843–851.
[6] U.H. Kurzweg, Enhanced heat conduction in oscillatory flow within parallel channels, J. Fluid Mech. 156 (1985) 291–300.
[7] U.H. Kurzweg, Enhanced heat conduction in fluid subjected to sinusoidal oscillations, J. Heat Transfer (ASME) 107 (1985) 459–462.
[8] U.H. Kurzweg, Temporal and spatial distribution of hear flux in oscillating flow subject to an axial temperature gradient, Int. J. Heat Mass Transfer 29 (12) (1986) 1969–1977.
[9] B.J. Bellhouse, R.W. Lewis, A high efficiency membrane separator for donor plasmapheresis, Trans. Am. Soc. Artif. Int. Org. 34 (1988) 747–754.
[10] H.R. Millward, B.J. Bellhouse, I.J. Sobey, The vortex wave membrane bioreactor: hydrodynamics and mass transfer, Chem. Eng. J. 62 (1996) 175–181.
[11] H.G. Gomaa, Al-Taweel, Intensification of inter-phase mass transfer: the combined effect of oscillatory motion and turbulence promoters, Heat Mass Transfer 43 (2007) 371–379.
[12] C. Herman, E. Kang, Comparative evaluation of three heat transfer enhancement strategies in a grooved channel, Heat Mass Transfer 37 (2001) 563–575.
[13] C. Herman, E. Kang, Experimental visualization and temperature field and study of heat transfer enhancement in oscillatory flow in a grooved channel, Heat Mass Transfer 37 (2001) 87–99.
[14] X. Ni, M.R. Mackley, A.P. Harvey, P. Stonestreet, M.H.I. Baird, N.V. Rama Rao, Mixing through oscillations and pulsations – A guide to achieve process enhancements in the chemical and process industries, Trans. Inst. Chem. Eng. 81 (2003) 373–383.
[15] M.R. Mackley, P. Stonestreet, Heat transfer and associated energy dissipation for oscillatory flow in baffled tubes, Chem. Eng. Sci. 50 (14) (1995) 2211–2224.
[16] M.E. Ralph, Oscillatory flow in wavy-walled tubes, J. Fluid Mech. 168 (1986) 515–540.
[17] M. Mackley, Use of oscillatory flow to improve performance, Chem. Eng. 43 (1986) 18–20.
[18] B.B. Gupta, J.A. Howell, D.X. Wu, R.W. Field, Helical baffle in cross flow microfiltration, J. Membr. Sci. 102 (1995) 31–42.
[19] V.G. Rodgers, R.E. Sparks, Reduction of membrane fouling in the ultrafiltration of binary protein mixtures, AIChE J. 37 (1991) 1517–1528.

[20] V.G. Rodgers, K.D. Miler, Analysis of steric hindrance reduction in pulsed protein ultrafiltration, J. Membr. Sci. 85 (1993) 39–58.
[21] K. Abel, Influence of oscillatory flows on protein ultrafiltration, J. Membr. Sci. 133 (1997) 39–55.
[22] T. Nishimura, K. Kunitsugu, A.M. Morega, Fluid mixing and mass transfer enhancement in grooved channels for pulsatile flow, J. Enhanc. Heat Transfer 5 (1998) 23–37.
[23] T. Nishimura, N. Oka, Y. Yoshinak, K. Kunitsugu, Influence of imposed oscillatory frequency on mass transfer enhancement of grooved channels for pulsatile flow, J. Heat Mass Transfer 43 (2000) 2365–2374.
[24] M. Yoshida, A. Ishita, K. Kinoshita, H. Miyashita, Heat transfer enhancement with an inclined semi-cylindrical turbulence promoter, Heat Transfer Jpn. Res. 26 (5) (1997) 332–344.
[25] N. Xu, W. Xing, N. Xu, J. Shi, Study on ceramic membrane bioreactor with TP, Sep. Purif. Technol. 32 (2003) 403–410.
[26] D.M. Krstic, M.N. Tekic, M.D. Caric, S.D. Milanovic, The effect of TP on cross-flow microfiltration of skim milk, J. Membr. Sci. 208 (2002) 303–314.
[27] H.G. Gomaa, A.M. Al-Taweel, Dynamic analysis at vertically oscillating surfaces, Chem. Eng. J. 102 (2004) 71–82.
[28] I.J. Sobey, On the flow through furrowed channels. Part 1. Calculated flow patterns, J. Fluid Mech. 96 (1980) 1–26.
[29] I.J. Sobey, The occurrence of separation in oscillatory flow, J. Fluid Mech. 134 (1983) 247–257.
[30] B.J. Bellhouse, F.H. Bellhouse, C.M. Curl, T.I. MacMillan, A.J. Gunning, E.H. Sparatt, S.B. MacMuurray, J.M. Nelems, A high efficiency membrane oxygenarator and pulsatile pumping system, and its application to animal trials, Trans. Am. Soc. Artif. Org. 19 (1973) 77–79.
[31] T. Howes, M.R. MacKley, E.P.L. Roberts, The simulation of chaotic mixing and dispersion for periodic flows in baffled channels, Chem. Eng. Sci. 46 (1994) 1669–1677.
[32] Y. Wang, J.A. Howell, R.W. Field, D. Wu, Simulation of cross-flow filtration for baffled tubular channels and pulsatile flow, J. Membr. Sci. 95 (1994) 243–258.
[33] T. Nashimura, N. Kojima, Mass transfer enhancement in symmetric sinusoidal wavy walled channel for pulsatile flow, Int. J. Heat Mass Transfer 38 (1995) 1719–1731.
[34] T. Nashimura, S. Matsune, Mass transfer enhancement in a sinusoidal wavy channel for pulsatile flow, Heat Mass Transfer 32 (1996) 65–72.
[35] T. Nashimura, Y.N. Bian, Y. Matsumoto, K. Kunitsugu, Fluid flow and mass transfer characteristics in a sinusoidal wavy-walled tube at moderate Reynolds numbers for steady flow, Heat Mass Transfer 39 (2003) 239–248.
[36] T. Nashimura, Y.N. Bian, K. Kunitsugu, Mass transfer characteristics in a sinusoidal wavy-walled tube by imposed fluid oscillation, AIChE J. 50 (2004) 762–770.
[37] H. Nagaoka, T. Nakano, D. Akimoto, Modeling of mass transfer in biofilms in oscillatory flow conditions using k–ε turbulence model, Water Sci. Technol. 3 (1) (2003) 201–207.
[38] N.V. Rama Rao, M.H.I. Baird, Heat transfer in a reciprocating plate column, Can. J. Chem. Eng. 78 (2000) 1056–1064.
[39] H. Schlichiting, Boundary-Layer Theory, seventh ed., McGraw-Hill Book Company, New York, 1979, p. 93.
[40] J. Nikuradse, Strmungsgesetze in Rauhen Rohren, Forschg. Arbein Ing.-Wesen, July/August, 1933, p. 361.
[41] H. Schlichiting, Boundary-Layer Theory, seventh ed., McGraw-Hill Book Company, New York, 1979, pp. 615–626.
[42] J. Tani, Turbulent boundary layer development over rough surfaces, in: H.U. Meier, P. Bradshaw (Eds.), Perspective in Turbulence Studies, Springer, 1987, pp. 223–249.
[43] A. Sigal, J.E. Danberg, New correlation of roughness density effect on the turbulent boundary layer, AIAA J. 28 (3) (1990) 554–556.
[44] P.H. Calderbank, M.B. Moo-Young, The continuous phase heat and mass-transfer properties of dispersions, Chem. Eng. Sci. 16 (1961) 39–54.
[45] Y. Kawase, M.B. Moo-Young, Solid-Turbulent fluid heat and mass transfer: A unified model on the energy dissipation rate concept, Chem. Eng. J. 36 (1987) 31–40.
[46] T.M. Liou, Y. Change, D.W. Hwang, Experimental and computational study of turbulent flows in a channel with two pairs of turbulent promoters in tandem, J. Fluid Eng. 112 (1990) 302–310.
[47] T.M. Liou, J.J. Hwang, S.H. Change, Simulation and measurement of enhanced turbulent heat transfer in a channel with periodic ribs on one wall, Int. J. Heat Mass Transfer 36 (1993) 507–517.
[48] S. Leonardi, P. Orlandi, R.J. Smalley, L. Djenidi, A.A. Antonia, Direct numerical simulation of turbulent channel flow with transverse square bars on one wall, J. Fluid Mech. 491 (2003) 229–238.